## PAPER

Check for updates

# Synthesis of polyaniline-encapsulated silver nanocomposites to improve removal efficacy of anti-alzheimer drug from aqueous solution and evaluation of their antioxidant properties†

Priya Kaushik,[a] Ruchi Bharti,*[a] Renu Sharma[a] and Annu Pandey (iD) *[b]

This study presents the synthesis of polyaniline-coated silver (PANI-Ag) nanocomposites *via in situ* oxidative polymerization and their application in the removal of piracetam, an anti-Alzheimer drug, from aqueous solutions. The nanocomposites were characterized using XRD, FTIR, SEM-EDX, DLS, UV-Vis, and HRTEM. Adsorption experiments optimized key parameters, including pH (7), drug concentration (800 ppm), contact time (180 min), and temperature (65 °C), achieving a 99% removal efficacy. Kinetic and isotherm studies confirmed a Langmuir monolayer adsorption model with pseudo-second-order kinetics, indicating chemisorption. Additionally, the antioxidant activity of PANI-Ag nanocomposites was evaluated using DPPH (56.42%) and ABTS (76.43%) assays, demonstrating superior free radical scavenging compared to PANI alone. These findings highlight the dual potential of PANI-Ag nanocomposites as efficient drug removal agents and antioxidant materials, offering promising applications in environmental remediation and biomedical fields.

### Environmental significance

Pharmaceutical residues such as piracetam, a commonly used anti-Alzheimer drug, are emerging contaminants increasingly detected in aquatic environments due to their incomplete removal by conventional treatment systems. This study introduces a green and scalable route for synthesizing polyaniline-encapsulated silver nanocomposites (PANI-Ag NCs) using garlic extract, which serves as both a reducing and stabilizing agent. The resulting nanocomposites demonstrate exceptional drug adsorption efficiency (up to 99%) and significant antioxidant activity, offering a dual-functional solution for wastewater remediation. By combining the high conductivity and adsorption capacity of polyaniline with the catalytic properties of silver nanoparticles, this eco-friendly material addresses pharmaceutical pollution while minimizing environmental toxicity typically associated with traditional nanomaterial synthesis. The work aligns with global sustainability goals, particularly SDG 6 (Clean Water and Sanitation) and SDG 12 (Responsible Consumption and Production), underscoring its relevance for future water purification technologies and green chemistry innovations.

## 1. Introduction

Water contamination is an escalating environmental issue, driven by industrial waste, pharmaceuticals, and toxic chemicals that persist in aquatic ecosystems.[1] Among these, pharmaceutical pollutants are of particular concern as they accumulate in water bodies, posing risks to both human health and aquatic life.[2–4] The detection of pharmaceutical pollutants even at low concentration in the aquatic environments highlights the critical need for efficient removal methods. Conventional water treatment methods, such as adsorption,[5] oxidation-

reduction,[6] membrane filtration,[7,8] and coagulation–flocculation,[9,10] have been employed to mitigate pollution, but these approaches are often inefficient, expensive, or unable to completely remove pharmaceutical residues.[11] These challenges highlight the need for cost-effective and efficient materials, such as polyaniline-silver nanocomposites, to advance the removal of pharmaceutical contaminants from water.[12]

One such pollutant, piracetam, a widely used nootropic drug, has been detected in wastewater.[13] Piracetam residues in water may interfere with the nervous systems of aquatic organisms, and could lead to long-term accumulation and increased antibiotic resistance.[14] These risks highlight the importance of removing piracetam from wastewater. Existing removal techniques, including ion exchange,[13] electrochemical processes,[15] and filtration,[16] often fail to achieve complete elimination.[17] This growing concern underscores the need for innovative, cost-effective, and sustainable solutions for pharmaceutical wastewater treatment.

*a*Department of Chemistry, University Institute of Sciences, Chandigarh University, Punjab, India. E-mail: ruchi.uis@cumail.in

*b*Department of Fibre and Polymer Technology, KTH Royal Institute of Technology, Stockholm, Sweden. E-mail: annua@kth.se

Nanotechnology offers a promising path forward, with materials such as silver nanoparticles (Ag NPs) demonstrating antibacterial properties, catalytic activity, and efficient pollutant removal.[18] However, conventional synthesis methods rely on toxic chemicals, which can be harmful to the environment.[19] A greener alternative involves the biosynthesis of nanoparticles using plant extracts, which act as natural reducing and stabilizing agents.[20,21] Garlic (*Allium sativum* L.), a well-known medicinal plant, has gained attention for its strong antioxidant and antimicrobial properties[22–24] and has been successfully employed in the green synthesis of silver nanoparticles, eliminating the need for hazardous reagents.[25] Recent studies, including the use of Equisetum diffusum extract for silver nanoparticle synthesis with selective $Hg^{2+}$ sensing and antimicrobial effects, highlight the increasing focus on eco-friendly, plant-based methods, supporting our garlic extract-mediated approach.[26]

Another key material in environmental remediation is polyaniline (PANI), a conductive polymer known for its high, environmental stability, electrical conductivity and high adsorption capability due to the presence of reactive amine and imine group that are capable of interacting with pollutant molecules.[27] Polyaniline exhibits similar functional properties to stimuli-responsive polymers, such as hydroxypropyl cellulose-succinate-salicylate, which shows pH- sensitive swelling and controlled pollutant interaction.[28] This highlights the potential to enhance PANI-based materials for improved environmental remediation and pollutant removal. Silver Nanoparticles (Ag NPs) possess a high surface area along with strong antimicrobial and catalytic properties, which make them suitable for applications in environmental and biomedical fields. Moreover, silver nanoparticles are widely employed to modify electrodes for sensitive and selective electrochemical detection of environmental pollutants. This modification improves electron transfer and signal response, enhancing their effectiveness in pollutant detection and remediation.[29] By combining PANI with silver nanoparticles, PANI-Ag nanocomposites offer a synergistic approach to pollutant removal, capitalizing on the adsorption efficiency of polyaniline and the catalytic potential of silver.[30,31]

As part of our research on sustainable solutions,[32–38] this study aims to synthesize eco-friendly, plant-mediated method to synthesize polyaniline-encapsulated silver nanocomposites (PANI-Ag NCs) using garlic extract and assess their effectiveness in removing piracetam drug from aqueous solutions. Our objective was to evaluate their efficiency in removing piracetam from aqueous solutions while also assessing their antioxidant properties. This research not only contributes to sustainable water treatment strategies but also aligns with global Sustainable Development Goals (SDGs), particularly SDG 6 (Clean Water & Sanitation), SDG 12 (Responsible Consumption & Production), SDG 9 (Industry, Innovation & Infrastructure), and SDG 13 (Climate Action).[39]

By developing environmentally friendly nanomaterials, this study provides a practical, scalable solution for tackling pharmaceutical pollution and highlights the potential biomedical applications of PANI-Ag nanocomposites.

# 2. Experimental methodology

## 2.1. Chemicals and materials

High-purity chemicals (>99%) were used, including aniline (monomer), hydrochloric acid, ammonium persulfate (APS), silver nitrate, fresh *Garlic*, double-distilled water, piracetam drug, 0.1 M HCl, and 0.1 M NaOH. Equipment included a pH meter, 0.001 g accuracy scale balance, 1000 μm micropipette, and cuvettes.

## 2.2. Preparation of garlic extract

20 grams of fresh garlic were obtained from a local market in Chandigarh. After thorough rinsing with double-distilled water to remove surface impurities, the *Garlic* was finely ground using a mortar and pestle. The grinded *Garlic* was immersed in 400 ml of double-distilled water and boiled at 100 °C until the solution underwent a colour change and volume of solution was reduced by half. After cooling to room temperature, the extract was filtered by using Whatman filter paper to obtain a clear garlic extract (G.E.) solution. This extract was employed as a reducing agent for the fabrication of silver nanoparticles.

## 2.3. Synthesis of polyaniline

To synthesize polyaniline, dispense 0.1 M Ammonium persulfate (APS) solution from a burette and titrate it against a 0.1 M Aniline solution that is prepared in 0.1 M hydrochloric acid (HCl) solution with continuous magnetic stirring. Allow the reaction to proceed for at least 5–6 hours at room temperature.[40]

## 2.4. Green synthesis of silver nanoparticles

A 0.1 M silver nitrate solution was prepared and titrated against 50 ml of *garlic extract* under continuous magnetic stirring at room temperature. After 20–25 minutes, the solution changed its colour from milky white to a milky pale-yellow colour precipitate, indicating the fabrication of silver nanoparticles. This method enables the reduction of $Ag^+$ ions to form silver nanoparticles within the *Garlic extract* solution.[41]

## 2.5. Fabrication of polyaniline based silver-nanocomposites

PANI-coated silver nanocomposites were synthesized by slowly adding silver nanoparticle solution dropwise into the freshly synthesized PANI solution (1 : 1 ratio) under continuous stirring at room temperature. The colour changes observed during the reaction of PANI-Ag NCs. The reaction proceeded for 24 hours to ensure uniform incorporation of Ag NPs into PANI. After 24 hours, product was centrifuged at 3000 rpm for 15 minutes to separate the nanocomposites. In this process, nanoparticles precipitated out from the solution, and the residual solution removed. The obtained nanoparticles were rinsed several times with double-distilled water and ethanol for removing any leftovers impurity and unreacted materials; hence, a high purity silver nanoparticle.

The final product was placed in an oven to dry at 60 °C for 12 hours to yield the PANI-coated silver nanocomposites. Then, the nanocomposites were kept in a desiccator for further

© 2025 The Author(s). Published by the Royal Society of Chemistry

*Environ. Sci.: Adv.*, 2025, **4**, 1250–1266 | **1251**

characterization and evaluation of their ability to remove pharmaceutical contaminants from aqueous solutions.

# 3. Characterization studies

After the successful synthesis of PANI-encapsulated silver nanocomposites using garlic extract, the nanocomposites were analyzed using various scientific instruments, which provided detailed confirmation of their structural, morphological, and compositional characteristics.

## 3.1. UV-visible spectral analysis

UV-Vis spectrophotometry is one of the most significant techniques to confirm the existence of metal nanoparticles in a liquid medium and to access their optical properties. The observed colour change, which implies the fabrication of PANI-coated silver nanocomposites, was further analyzed with the help of a UV-Vis spectrophotometer.

We used a Shimadzu UV-1900 UV-VIS spectrophotometer to analyze their absorption and transmission of light in samples.

The UV-Vis spectra for garlic extract, silver nanoparticles, polyaniline (PANI), and polyaniline-coated silver nanocomposites were obtained as illustrated in Fig. 1. Each sample was analyzed over the complete wavelength range of 200 to 800 nanometers at ambient temperature.

The black curve represents the garlic extract, showing, which shows a baseline absorbance that does not exhibit sharp, prominent peaks, which corresponds to the adsorption of bioactive compounds present in the garlic extract. The red curve confirms the presence of Ag NPs with the 258 nm region showing the electronic transition of silver nanoparticles in UV region, while the 410 nm is another characteristic SPR peak (Surface Plasmon Resonance Peak) found in the visible range. Singh *et al.* reported synthesis of Ag nanoparticles which matches the result of our current finding.[42] The blue curve shows peaks near 235 nm, corresponding to $\pi$–$\pi$ transition of

benzenoid rings* and around 286 nm, related to the $\pi$–$\pi$ transition of quinoid rings*, confirming the presence of Polyaniline. The green curve confirms the presence of both PANI and Ag NCs, with the 240–290 nm region showing $\pi$–$\pi$* transitions from the PANI structure, while the SPR peak around 434 nm from Ag NCs becomes less prominent, indicating the successful integration of silver nanoparticles into the PANI matrix. Verma *et al.* reported the fabrication of Cu-doped PANI nanocomposite in 2024 which matches the UV-range observed in our current finding.[43]

## 3.2. FTIR spectral analysis

FTIR spectroscopy was carried out using the PerkinElmer Fourier-Transform Infrared Radiation spectrophotometer, range between 4000 cm$^{-1}$ and 400 cm$^{-1}$, well known for its exceptional optical performance and study the chemical bonds present in the nanoparticles and nanocomposites. Fig. 3 illustrates the FTIR spectrum of Polyaniline and Polyaniline-coated silver nanocomposites fabricated using *Garlic extract*. In Fig. 2(a), the absorption peaks are located mainly at 2981 cm$^{-1}$, 1587 cm$^{-1}$, 1495 cm$^{-1}$, 1296 cm$^{-1}$, 1148 cm$^{-1}$, 817 cm$^{-1}$ in the region 4000 cm$^{-1}$ to 400 cm$^{-1}$.

The prominent peak at 2981 cm$^{-1}$ in an IR spectrum is typically associated with the stretching vibration of C–H bonds of PANI. The peak at 1587 cm$^{-1}$ often corresponds to the C=C stretching vibrations in its quinonoid structure, whereas a peak at 1495 cm$^{-1}$ typically corresponds to the C=C stretching vibration in its benzenoid structure. The peak at 1296 cm$^{-1}$ in an IR spectrum often corresponds to C–N stretching vibrations. The peak at 817 cm$^{-1}$ in an IR spectrum often corresponds to the bending vibration of C–H bonds in substituted aromatic compounds or out-of-plane bending vibrations in aromatic rings. These results are aligned with the previous studies that had reported identical characteristics bands of polyaniline.[44]

In Fig. 2(b), The sharp peak at 3228 cm$^{-1}$ arises from the vibrational and deformational characteristics associated with N–H bonds. The peak at 1495 cm$^{-1}$ demonstrates the appearance of N–B–N structure, with B representing a benzene ring.
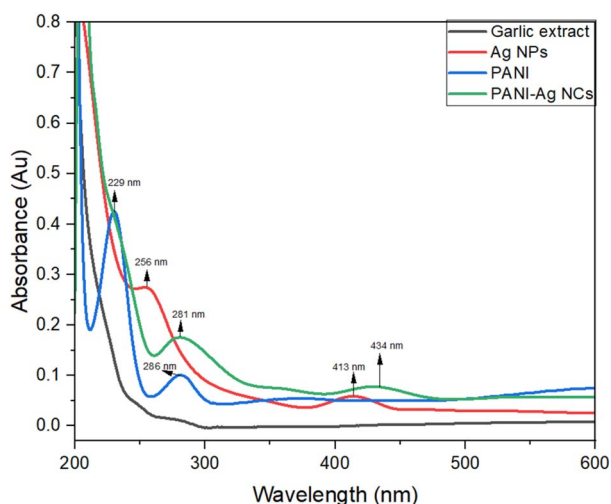


Fig. 1   UV spectrophotometer of G.E., silver nanoparticles, polyaniline, polyaniline-coated silver nanocomposites.
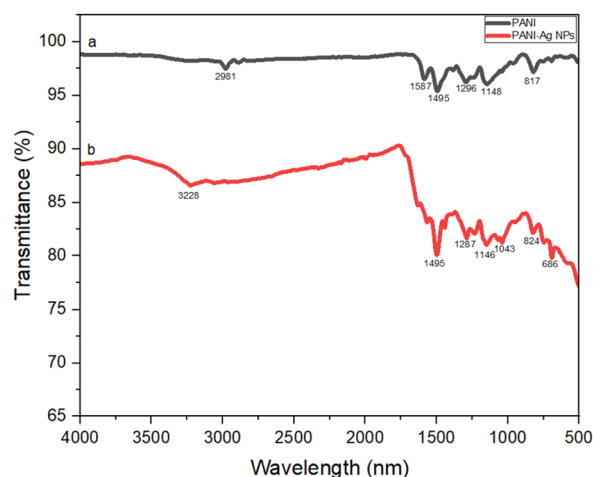


Fig. 2   (a) FTIR analysis of PANI (b) FTIR analysis of PANI-incapsulated silver nanocomposites.

The peak at 1287 cm$^{-1}$ and 1146 cm$^{-1}$ indicates the C–N stretching. The peak at 1043 cm$^{-1}$ the stretching vibrations of the C–O bond. The peak at 824 cm$^{-1}$ indicates the bending vibrations in C–H bond in an aromatic group. The peak at 686 cm$^{-1}$ indicates the Ag–N interaction confirming the corporation of silver nanoparticles in polyaniline. This peak act as a unique feature for the PANI component within the PANI-silver nanocomposites. These findings were consistent with the results of earlier studies,[45] which had reported similar characteristics bands for Polyaniline-silver nanocomposites (PANI-Ag NCs).

### 3.3. X-ray diffraction analysis

We used an analytical X'PERT PRO X-ray diffractometer (XRD) to record the X-ray diffraction patterns. Fig. 3(a) illustrated the characteristic X-ray diffraction patterns of Polyaniline. This pattern has two clear and sharp peaks at $2\theta = 20°, 25°$ which demonstrates the existence of (110) and (200) planes, respectively. The X-ray diffraction pattern of PANI has a crystallinity of 39.4% and 60.6% amorphous. By employing Debye–Scherrer formula, we calculated the crystal size of PANI as 16.27 nm.

Fig. 3(b) illustrated the characteristics X-ray diffraction patterns of polyaniline-coated silver nanocomposites. This pattern has 6 sharp peaks at $2\theta = 28.2°, 32.7°, 38.6°, 46.6°, 55.2°,$ and $57.9°$. The peaks at 28.2° and 32.7° are uncommon in typical silver XRD pattern. It might indicate the presence of other phase or the extra interaction between PANI and Silver. The main peaks at 38.6°, 46.6°, 55.2°. These findings are aligned with the previous study which has reported the synthesis of polyaniline/silver nanocomposites.[46] The diffraction analysis of PANI-Ag NCs showed the crystallinity of 71.9% and 24.12% amorphous. The crystal size of PANI-Ag Cs was determined to be 28.77 nm which confirmed the presence of well-defined crystalline structure.

The crystallite size ($D$) can be determined using the Debye–Scherrer formula:

$$\text{Crystal size}(D) = \frac{K\lambda}{\beta \cos \theta}$$

$K$ denotes the shape factor, set at a specific value of 0.94 for this analysis. $\lambda$ represents the wavelength of the incident Cu–K$\alpha$ X-ray radiation, precisely 0.154252 nm. $\beta$ indicates the full width at half maximum (FWHM), measured in radians. $\theta$ refers to Bragg's angle, also expressed in radians.

### 3.4. Scanning-electron microscopy with energy dispersive X-ray spectroscopy (SEM-EDX)

We examined the structure and surface properties of PANI, silver nanoparticles and PANI-Silver nanocomposites using the HITACHI SUB080 SERIES microscope for SEM-EDX.

We conducted Morphology analysis and particle size and composition of PANI, Ag NPs and PANI-silver nanocomposites in sample by integrating scanning electron microscopy with energy dispersive X-ray spectroscopy (SEM-EDX).

Fig. 4 illustrated the SEM image, providing an in-depth examination of the surface morphology and shape of the Polyaniline, silver nanoparticles and Polyaniline-coated silver nanocomposites. This technique provides a great way of viewing three-dimensional surface features; high-resolution images are availed that enable the identification of important features such as particle size and shape, surface roughness, among others. It is through such observations that one is able to get an insight into the structural aspects of the material being handled. Notably, the analysis indicates that the SEM image of PANI shows large and irregular shape particles with rough and porous surfaces. Silver NPs shows the irregular spherical shape and the PANI-coated silver nanocomposites display a non-porous structure with an irregularly spherical morphology.

SEM-EDX analysis of the synthesized nanoparticles confirms the successful formation of polyaniline-coated silver nanocomposites. The elemental composition of the fabricated PANI-coated Ag nanocomposites, which included carbon (C), nitrogen (N), oxygen (O), and silver (Ag), was verified by EDX analysis. The major element was silver, which had a mass percentage of 72.42 ± 3.79% and an atom percentage of 26.19 ± 1.37%. Both nitrogen and oxygen made significant contributions: nitrogen made up 8.92 ± 1.67% of the mass and 24.85 ±
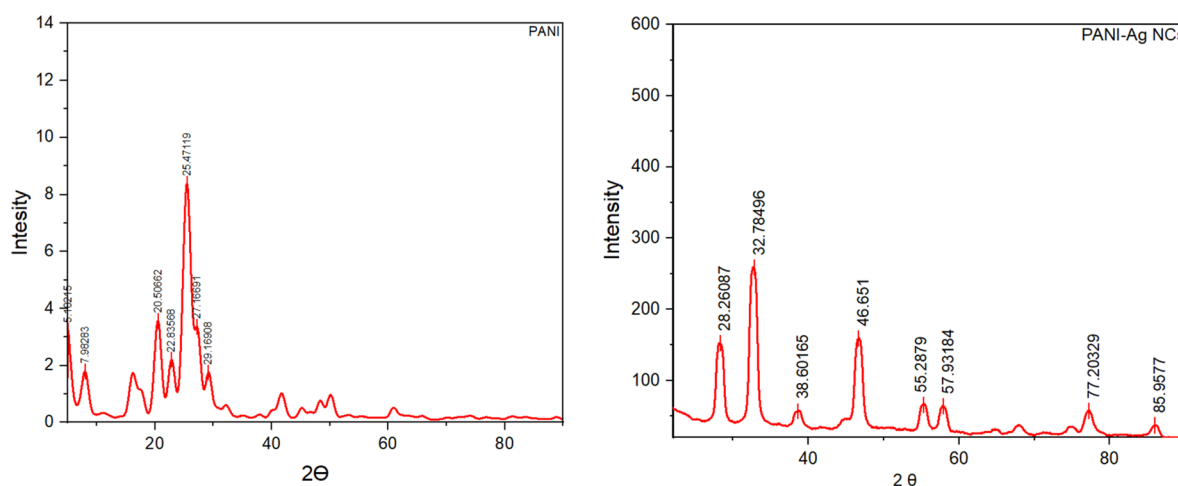


**Fig. 3** X-ray diffraction analysis of synthesized PANI & PANI-coated silver nanocomposites.

© 2025 The Author(s). Published by the Royal Society of Chemistry

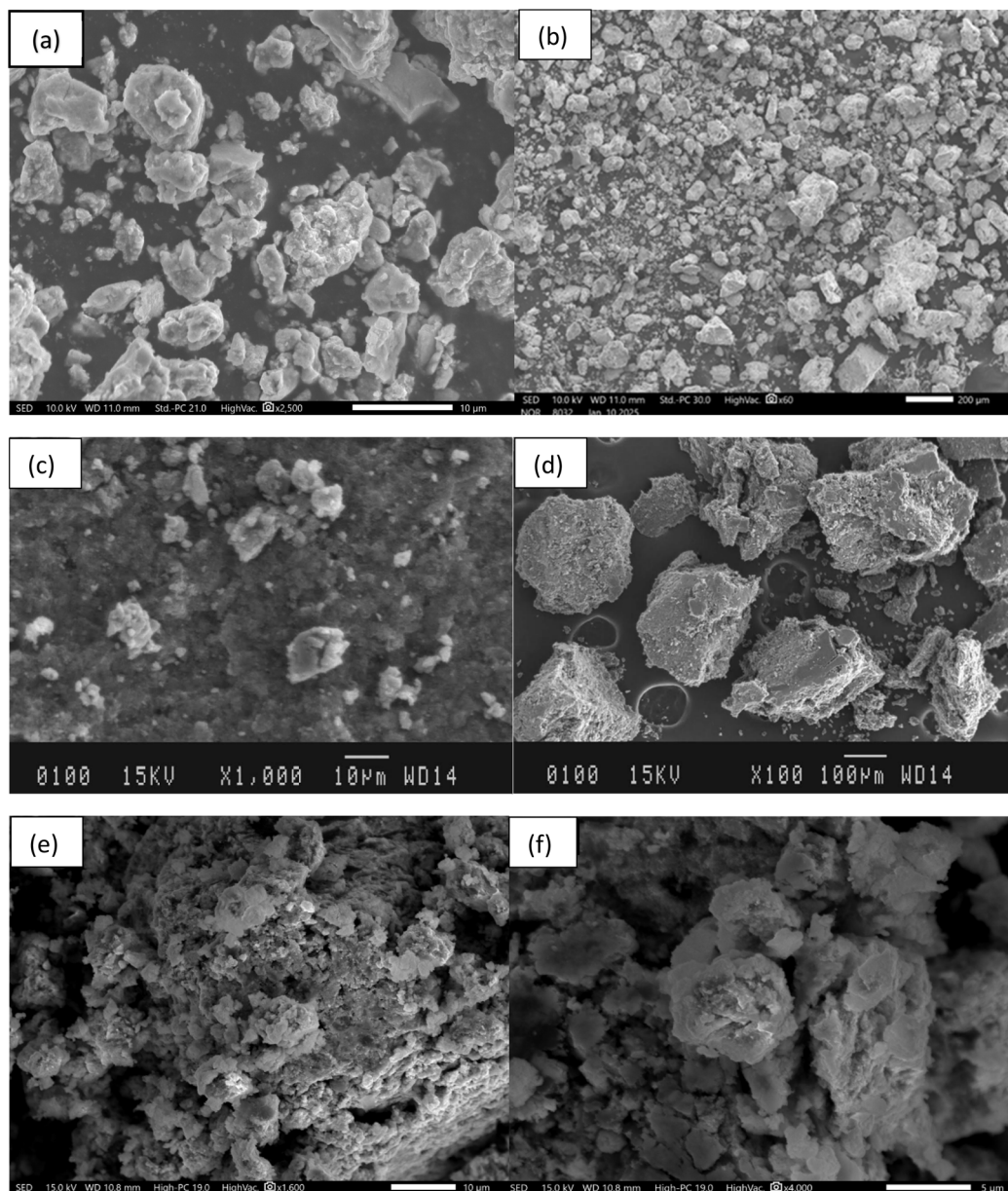*Environ. Sci.: Adv.*, 2025, **4**, 1250–1266 | **1253**

**Fig. 4** SEM image of synthesized (a) & (b) silver nanoparticles (c) & (d) PANI (e) & (f) PANI-coated silver nanocomposites.

4.66% of the atom, while oxygen made up $14.37 \pm 2.05\%$ of the mass and $35.04 \pm 4.99\%$ of the atom. At a mass percentage of $4.28 \pm 0.37\%$ and an atom percentage of $13.92 \pm 1.21\%$, carbon was less prevalent. The average size of the nanoparticles was also determined using ImageJ software, and it was found to be 48 nm. Mehdi Rezvani *et al.* reported the synthesis of PANI-magnetite nanocomposites and reported the average size as 40 nm, validating our current findings.[47]

### 3.5. High resolution transmission electron microscopy (HRTEM)

The successful synthesis of PANI-Ag NCs is verified by high-resolution transmission electron microscopy (HRTEM) analysis. The HRTEM image of the PANI-Ag NCs is depicted in Fig. 8. It provides detailed structural information concerning the

formation and morphology at the nanoscale. The silver nanoparticles exhibit a spherical or slightly irregular morphology, with well-defined edges. A thin layer, likely the polyaniline (PANI) coating, is visible. The uniformity of this coating indicates successful incorporation of silver nanoparticles by PANI.[48] The HRTEM images of the polyaniline/Ag nanocomposites as shown in Fig. 5 revealed that the silver nanoparticles are evenly distributed within the Polyaniline matrix. As shown by these HRTEM images of the current composite, silver nanoparticles feature as dark, nearly spherical dots on the smooth, bright polyaniline coating shell surface.

### 3.8. Thermal behavior and stability: comparative insight

While the present study primarily focused on the synthesis, characterization, and functional performance of the PANI-Ag
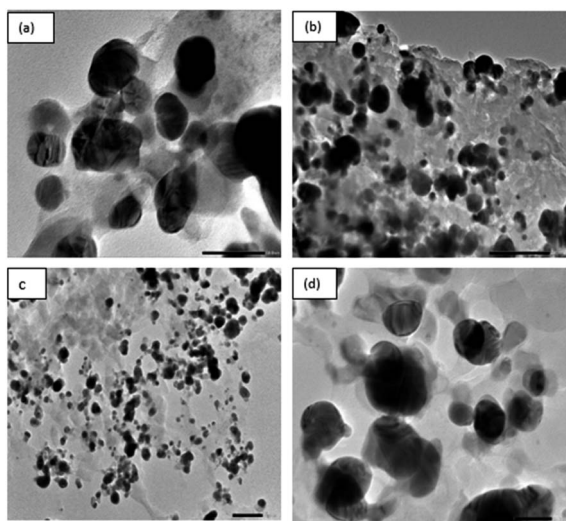
Fig. 5 (a–d) High resolution transmission electron microscopy (HRTEM) images of the synthesized PANI-Ag nanocomposites.

**Table 1** DLS data for synthesized PANI-Ag NCs

| | |
|---|---|
| Hydrodynamic diameter | 285.6 nm |
| Polydispersity index | 0.25 |
| Diffusion coefficient | 0.8 µm2/s |
| Intercept $g_1^2$ 0.6866 | 0.6866 |
| Fit error | 0.0001997 |
| Peak intensity 1 | 163.92 nm |
| Peak intensity 2 | 636.83 nm |

nanocomposites, it is important to consider the thermal stability of such materials, especially for their potential application in biomedical and environmental settings. Although thermogravimetric or calorimetric analysis was not conducted in this work, existing literature provides supportive insights. For instance, hydrogel matrices derived from Salvia spinosa seeds have demonstrated commendable thermal resistance and degradation kinetics, making them promising candidates for sustained drug release under varying conditions.[49] Considering the established thermal resilience of polyaniline and the stabilizing effects of silver nanoparticles, it is reasonable to anticipate that the synthesized nanocomposites possess favorable thermal behavior. Nonetheless, future studies will aim to incorporate comprehensive thermal profiling using TGA and DSC techniques to quantitatively assess stability under operational conditions.

### 3.6. Dynamic light scattering analysis (DLS)

The characterization of PANI-Ag-nanocomposites in this work provides important information on some of their physical and optical properties. The DLS analysis provides comprehensive insights into the size distribution, dispersion quality, and stability of the synthesized PANI-Ag nanocomposites. The size distribution graphs revealed a primary peak at about 163.92 nm, representing the most prevalent size of the nanoparticles, while a secondary peak at about 636.8 nm was found, indicating the presence of minor aggregation within the sample.

The hydrodynamic diameter was 285.58 nm, as shown in Table 1, reflecting the average dimension of nanoparticles in solution, including interaction with the surrounding medium. The poly dispersity Index (PDI) was 0.25 which indicates a moderately monodispersed system, which is typical for nanocomposites synthesized through green methods. The high mean intensity of 289.124 kcounts per s greatly signifies biomedical imaging because this was representative of the average scattered light detected. Increased visibility by nanoparticles increases

their chances of detection and analyses in biomedical imaging for increased image quality and sharpness in visual acuity. The total intensity of 139 677.9 kcounts per s clearly depicts the overview of the scattering properties of the silver nanoparticles and their interaction with the X-ray beam in the study. These findings had been consistent with the previous research, which validating the data reported by Sheeba Ghani *et al.* on the synthesis of Ag/PANI composite counter electrodes (CEs).[50]

### 3.7. Zeta-potential of PANI-Ag NCs

The zeta-potential of the synthesized PANI-Ag nanocomposites was measured to estimate their colloidal stability. A zeta potential value in the range of −20 to −30 mV suggests moderate stability because this magnitude indicates that electrostatic repulsion between the particles is sufficient to prevent aggregation. This stability is further enhanced by the capping agents from the plant extract, which help in maintaining the dispersion of the particles. As shown in Fig. 6, the PANI-coated silver nanoparticles showed a good stability due to the presence of their negative surface charge, given that the zeta potential was −21.84 mV. Ebrahim *et al.* in 2020 reported zeta potential of PANI/Ag/GO QD nanocomposite as 30.3 mV, which matches the result of synthesized PANI-Ag NCs, validating the synthesis process.[51]

## 4. Antioxidant studies

Antioxidants are crucial in preventing molecule oxidation and counteracting free radicals, protecting cells from oxidative stress. They help prevent damage to DNA, proteins, and lipids, contributing to overall health. Additionally, antioxidants may protect against chronic diseases, highlighting their broader health benefits. The antioxidant activity of Polyaniline and Polyaniline-coated silver nanocomposites were determined by DPPH (2,2-diphenyl-1-picrylhydrazyl) method and ABTS (2,2′-azinobis (3-ethylbenzothiazoline-6-sulfonic acid)) method. All antioxidant assays were conducted in triplicate to confirm the consistency and reliability of the results.

### 4.1. DPPH assay

In this assay, the DPPH radicals, which have a deep blue color in alcoholic solutions, react with visible changes in the presence of antioxidants. Antioxidants cause a noticeable color change to pale yellow or even colorless due to their fast action of reducing DPPH radicals by providing hydrogen atoms or electrons. The absorbance is observed at a wavelength of 517 nm.[52] The DPPH scavenging activity was calculated by following equation:
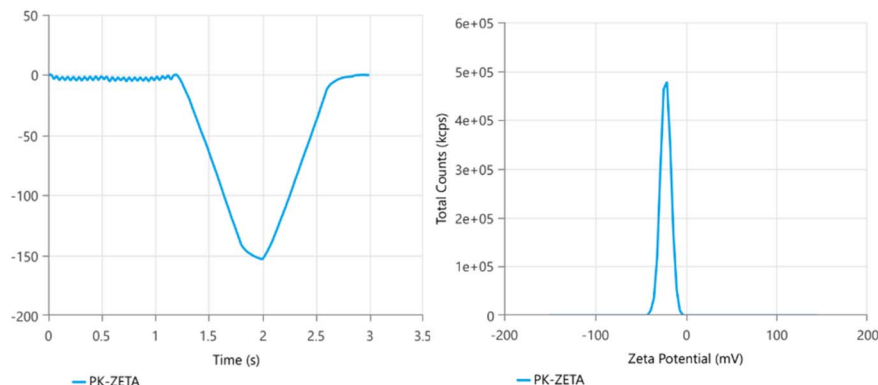
© 2025 The Author(s). Published by the Royal Society of Chemistry

*Environ. Sci.: Adv.*, 2025, **4**, 1250–1266 | **1255**

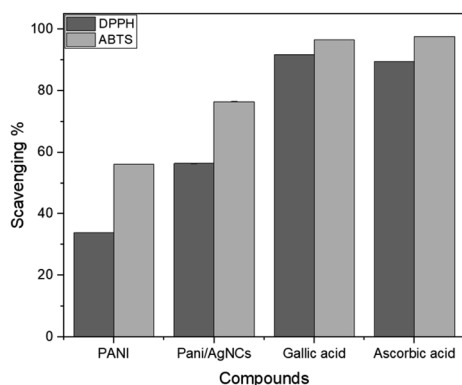**Fig. 6** Zeta potential distribution graph for synthesized PANI-Ag NCs.



**Fig. 7** Antioxidant activity comparison of PANI, PANI-Ag NCs, gallic acid and ascorbic acid.

$$*\text{DPPH scavanging \%} = \left[\frac{A_{\text{Control}} - A_{\text{sample}}}{A_{\text{Control}}}\right] \times 100$$

In this study, PANI showed a significant antioxidant activity as shown in Fig. 7, measured at $33.8 \pm 0.05\%$. The antioxidant activity of PANI-coated silver nanocomposites was improved to $56.16 \pm 0.14\%$ compared to standard solution like Gallic acid ($91.76 \pm 0.15\%$) and ascorbic acid ($89.52 \pm 0.09\%$). A decrease in absorbance directly represents the antioxidant activity of the tested compounds, since it is a function of radicals being neutralized by the antioxidant. Statical analysis showed that the antioxidant activity of PANI-coated silver nanocomposites was significantly higher than that of PANI alone ($p < 0.05$). The results suggest that the incorporation of silver nanoparticles enhances polyaniline's efficiency to scavenge radicals. This is possibly because the silver nanoparticles somehow combine synergistically with PANI, enhancing the ability to donate an electron or a hydrogen atom.

### 4.2. ABTS assay

The synthesized nanoparticles were evaluated using the ABTS cation radical technique, which measures antioxidant activity by reducing absorption at 734 nm. PANI showed significant antioxidant activity ($56.16 \pm 011\%$) The PANI-coated nanocomposites showed significant antioxidant activity ($76.70 \pm 0.14\%$) compared

to standards like Gallic acid ($96.93 \pm 0.25\%$) and ascorbic acid ($97.63 \pm 0.15\%$), indicating their potential in combating oxidative stress. PANI-coated silver nanocomposites exhibit higher antioxidant activity than PANI alone, emphasizing the benefits of nanocomposite formation. The antioxidant activity of the nanocomposites nevertheless remains lower than that of standard antioxidants despite of this improvement, indicating that PANI-based materials could potentially be employed as additional antioxidants but not as direct substitutes for prominent antioxidants like ascorbic acid and gallic acid. The ABTS scavenging activity was calculated by the equation as follows:

$$*\text{ABTS scavanging\%} = \left[\frac{A_{\text{Control}} - A_{\text{sample}}}{A_{\text{Control}}}\right] \times 100$$

Statical analysis confirmed the significant increase in antioxidant activity for PANI-coated silver nanocomposites compared to PANI and Ag NPs ($p < 0.05$). PANI-coated silver nanocomposites possess moderate-to-good antioxidant activity, making them promising materials for specific applications. However, their performance compared to gallic acid and ascorbic acid suggests that although they can complement traditional antioxidants, they are not yet a direct replacement. Additionally, multifunctional nanomaterials like sulfonamide-functionalized silver nanoparticles have demonstrated promising properties, including effective antioxidant activity, selective $Ni^{2+}$ sensing, and antimicrobial effects. This highlights the potential for combined applications and underscores the multifunctional benefits of silver-based nanocomposotes such as PANI-coated silver nanocomposites investigated in this study.[53] Recent studies have also reported the biomedical relevance of Ag NPs, including antimicrobial and wound healing applications.[54]

## 5. Applications of polyaniline-encapsulated silver nanocomposites for drug removal from aqueous solutions

The study on PANI-coated silver nanocomposites displayed promising applications of these nanomaterials in both
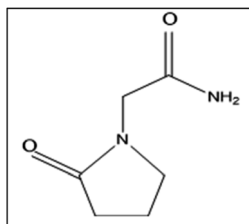
**Fig. 8** Structure of piracetam drug.

environments and the biomedical fields. These nanocomposites possess significant potential for removing drugs from aqueous solutions in the environmental domain, The Experimental investigations were carried out at a fixed room temperature *i.e.*, 25 °C. Piracetam has been selected for study due to its widespread incorporation into numerous industrial products. The chemical structure of Piracetam drug is illustrated in Fig. 8 as follows:

Throughout all experiments, the subsequent expressions were used to determine the percentage of Drug removal and the quantity of drug adsorbed at equilibrium.[55]

The percentage removal (%R) of the drug was determined by using the formula:

$$\% \, R = \frac{C_0 - C_e}{C_0} \times 100$$

where $C_0$ represents the initial concentration and $C_e$ represents the final concentration of the drug. To examine the adsorption capacity of the PANI-coated silver nanocomposites, the quantity of drug adsorbed ($Q_e$ in mg g$^{-1}$) was determined by employing the formula:

$$Q_e = \frac{(C_0 - C_e)V}{M}$$

In this equation, $C_0$ and $C_e$ are the initial and final drug concentrations (mg L$^{-1}$), respectively; $V$ is the volume of the solution in litters; and $M$ is the mass of PANI/Ag NCs used (g). The study focused on evaluating the efficiency of polyaniline-coated silver nanocomposites by examining how various physical parameters affect adsorption.

## 5.1. Effect of operational parameters on drug removal

Experimental investigations were conducted under controlled conditions, including varying pH, contact time, temperature,

and dosages of PANI-coated silver Nanocomposites. Table 2 presents the specific conditions analyzed for each parameter.

The results indicated that these nanocomposites can effectively remove Piracetam from aqueous solutions, with drug removal efficacy being influenced by the parameters studied.

**5.1.1. Effect of dose of adsorbent.** The dose of adsorbent in the adsorption process is an extensive factor that affected the rate of adsorption. The adsorption experiment was conducted using various dose of adsorbent *i.e.*, PANI-Ag NCs, ranging to the drug as shown in Fig. 10.

The magnetic stirring speed was maintained at 950 rpm, and the pH of the drug solution was regulated at 7. The findings of this research are illustrated in Fig. 9 from 10 mg to 30 mg, which were applied the drug. This variation can be observed in Fig. 9 where 10 and 20 mg of PANI-Ag NCs dose shows moderate drug removal efficacy by adsorption. When 30 mg of adsorbent was added, the removal efficacy of the PANI-Ag NCs increased. The results demonstrated that the adsorption efficiency is directly proportional to the quantity of adsorbent present in the drug solution. As the dose of the adsorbent increases, the rate of adsorption also increases. Consequently, as the dose of PANI-Ag NCs increases, the surface area available for interaction with the drug also expands, enhancing the overall adsorption rate.

**5.1.2. Effect of pH of drug solution.** In this study, the pH variation played a crucial role in influencing the removal efficacy. The adsorption experiment was conducted at 800 ppm drug concentration and a 30 mg dose of PANI-coated silver NCs, a contact time of 90 min, at room temperature, with pH conditions varied between acidic (pH = 2 and 4), neutral (pH = 7), and basic (pH = 10 and 12). The agitation speed was fixed at 960 rpm along the experiment. It can be found from Fig. 10 that changes in the pH value would affect the removal of the drug, with the highest removal occurring under a neutral environment at pH = 7.

The changes in the level of pH result in changes on the surface of the adsorbent, which again impact the efficiency in sorption. The effectiveness of removal was reduced at both acidic (pH 10 and 12) and basic (pH 2 and 4). At pH 2 and 4 as shown in Fig. 10(a and b), protonation of the adsorbent surface produced a positive charge, which leads to repulsion with positively charged drug molecules, reducing adsorption efficiency. Similarly, at pH 10 and 12 as shown in Fig. 10(d and e), Piracetam ionized into a negatively charged form and electrostatic repulsion with a negatively charged adsorbent reduced

**Table 2** Condition in the effect of each parameter

| Factors (range) | pH | Drug concentration (ppm) | Time (min) | Temperature (°C) |
|---|---|---|---|---|
| pH (2–10) | | 800 ppm | 90 min | 43 °C |
| Adsorbent dosage (10–30 mg) | 7 | 800 ppm | 90 min | 43 °C |
| Temperature (20–95 °C) | 7 | 800 ppm | 90 min | |
| Time (15–180 min) | 7 | 800 ppm | 180 min | 65 °C |
| Concentration (50–800 ppm) | 7 | | 180 min | 65 °C |

© 2025 The Author(s). Published by the Royal Society of Chemistry

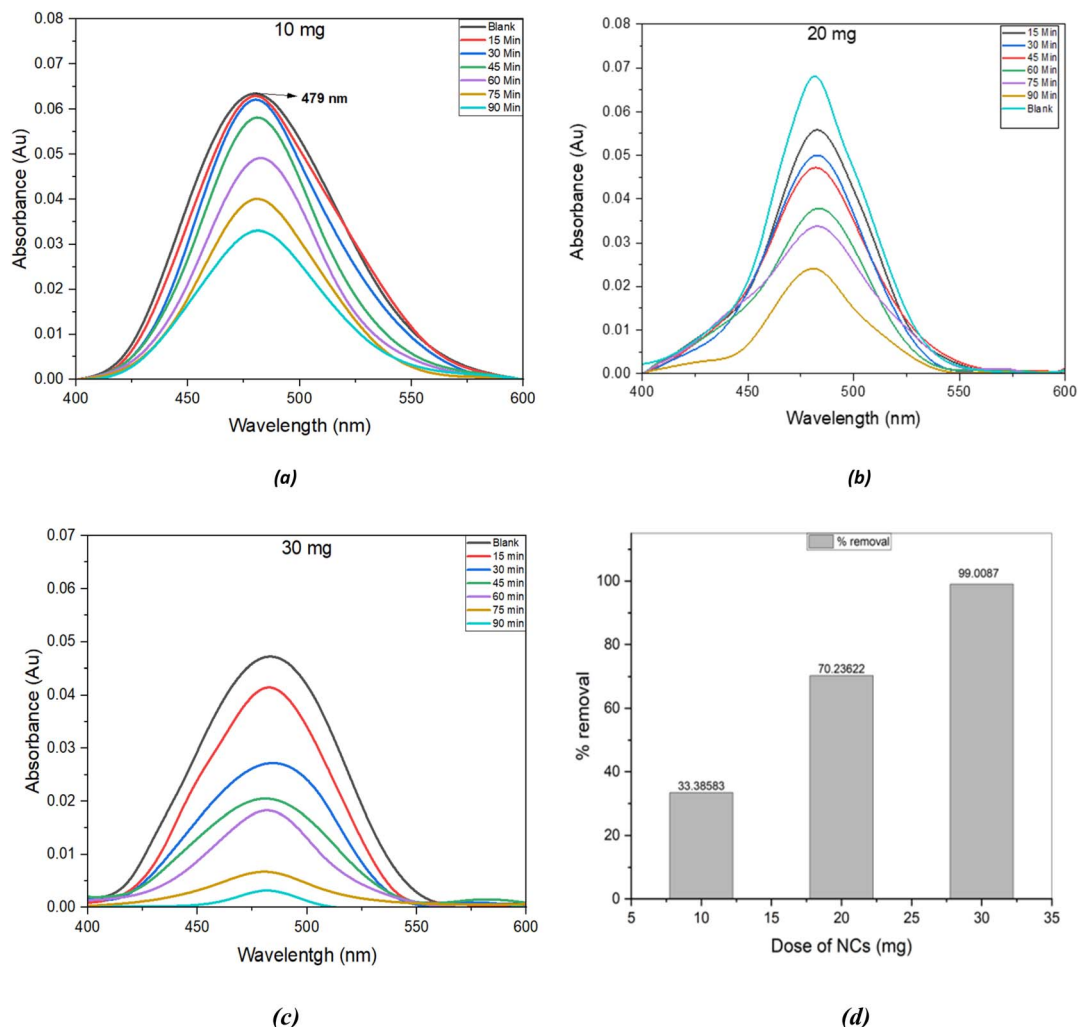*Environ. Sci.: Adv.*, 2025, **4**, 1250–1266 | **1257**

**Fig. 9** The effect of dose of adsorbent (PANI-Ag NCs) as (a) 10 mg, (b) 20 mg and (c) 30 mg under conditions of a drug solution concentration of 800 ppm, a contact time of 90 minutes, pH 7 and at room temperature, (d) Bar graph of adsorption of Piracetam at various doses by PANI-Ag NCs.

removal efficacy. Highest adsorption occurred at neutral pH 7 as shown in Fig. 10c, where electrostatic interactions were reduced.[56]

**5.1.3. Effect of temperature.** The adsorption experiment for the drug solution using the PANI-Ag nanocomposite adsorbent was performed by varying the temperature ranging from 20 °C to 95 °C, with a drug concentration of 800 ppm, at pH 7, and an adsorbent dose of 30 mg. The results, as depicted in Fig. 11, show that an increase in temperature increases the drug removal rate and deceases the absorbance, with this adsorption rate reaching an equilibrium at 65 °C for the adsorbent. At equilibrium, the amount of the drug being adsorbed onto the adsorbent becomes equal to the amount returned to solution, forming a steady-state condition. The thermal behaviour of the PANI-Ag nanocomposites indicates good stability under adsorption conditions, which underscores their potential effectiveness for use in environmental remediation and pharmaceutical applications, even under higher temperature conditions.[57]

**5.1.4. Effect of time.** The adsorption experiment for the drug solution with the PANI-Ag nanocomposite adsorbent was conducted by varying the contact time from 15 min to 180 minutes. The experiment was carried out with a drug concentration of 800 ppm, at pH 7, using an adsorbent dose of 30 mg, and a temperature of 65 °C. The agitation speed was fixed at 960 rpm along the experiment. The variations can be observed in Fig. 12 where the drug removal efficacy at 180 minutes showed a significant higher value. The result demonstrated that the drug removal efficacy of the drug increases with longer contact time. This indicates a positive correlation between contact time and the efficiency of drug adsorption by the adsorbent.

**5.1.5. Effect of concentration of drug solution.** To explore the adsorption capacity of synthesized PANI-coated Ag NCs, the adsorption experiment was performed with drug concentrations varying from 50 ppm to 800 ppm, at pH 7, using 30 mg of adsorbent at 65 °C temperatures in a contact time of 180 minutes. From Fig. 13, it was observed that 50 ppm
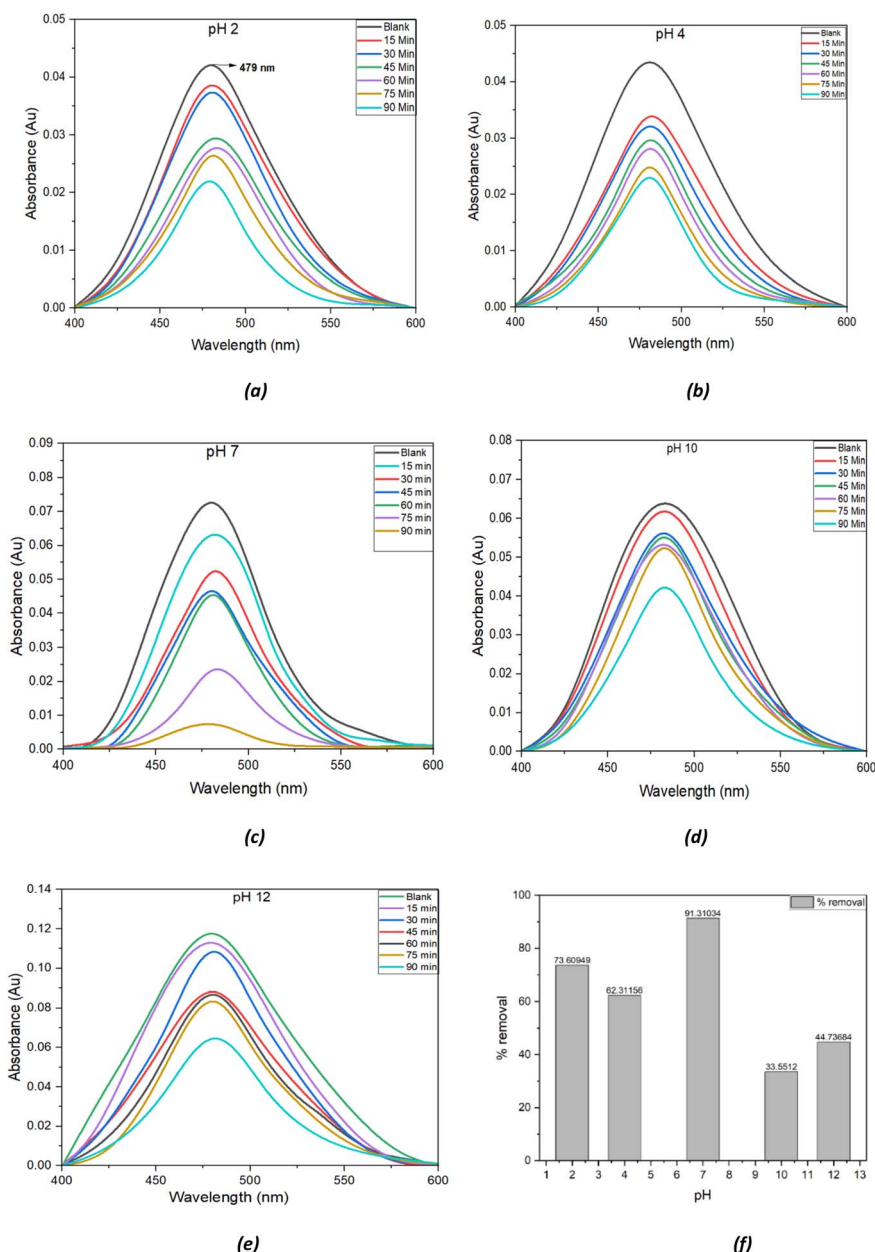
**1258** | *Environ. Sci.: Adv.*, 2025, **4**, 1250–1266

© 2025 The Author(s). Published by the Royal Society of Chemistry

**Fig. 10** (a–e) The effect of pH on drug removal was investigated under conditions of a drug solution concentration of 800 ppm, a contact time of 90 minutes, and an adsorbent dose of 30 mg, (f) bar graph of adsorption of Piracetam at various pH by PANI-Ag NCs.

concentration of drug solution showed less adsorption efficiency and 800 ppm concentration of drug solution of drug showed the higher drug removal efficacy. Fig. 13 depicted that the adsorption efficiency increases with increasing in drug concentration, likely due to the higher availability of drug molecules facilitating grater adsorption onto active sites.

### 5.2. Mechanism of piracetam adsorption onto PANI-Ag nanocomposites

The adsorption of piracetam onto PANI-coated silver nanocomposites is primarily governed by electrostatic interactions, hydrogen bonding, and π–π stacking. The presence of positively charged polyaniline (PANI) in acidic conditions facilitates adsorption by interacting with the negatively charged oxygen-containing functional groups in piracetam molecules. A schematic diagram of the adsorption mechanism, highlighting the key interactions responsible for effective drug removal as illustrated in Fig. 14. Additionally, silver nanoparticles enhance adsorption by providing active binding sites for drug molecules. The superior adsorption of PANI-Ag NCs arises from the synergistic effect between polyaniline and silver nanoparticles.[57]

The adsorption process follows a Langmuir monolayer model, indicating uniform surface adsorption without significant multilayer formation. Kinetic studies confirmed pseudo-second-order behaviour, suggesting a chemisorption
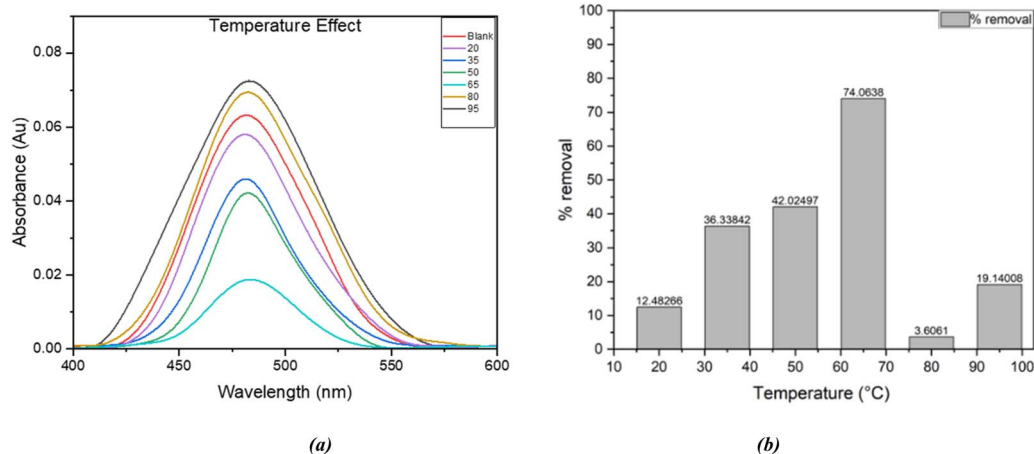
© 2025 The Author(s). Published by the Royal Society of Chemistry

*Environ. Sci.: Adv.*, 2025, **4**, 1250–1266 | **1259**

**Fig. 11** (a) The effect of temperature on drug removal was examined under constant conditions: a drug concentration of 800 ppm, an adsorbent dose of 30 mg, pH 7, and a contact time of 90 minutes, (b) bar graph of adsorption of Piracetam at various temperature.

mechanism, where electron exchange or covalent interactions play a role.

# 6. Kinetic and adsorption isotherms

The adsorption kinetics and isotherms of piracetam drug removal using polyaniline-coated silver (PANI-Ag) nanocomposites were evaluated systematically. The data provide essential insights into the adsorption mechanism, surface interactions, and equilibrium properties of the nanocomposites, ensuring an effective removal process.

### 6.1. Adsorption isotherm

In solid–liquid systems, the equilibrium of sorption is a key physico-chemical factor that helps explain the behavior of adsorption processes. Adsorption isotherms describe the relationship between the concentration of the substance being adsorbed in the solution and the amount that adsorbed at the
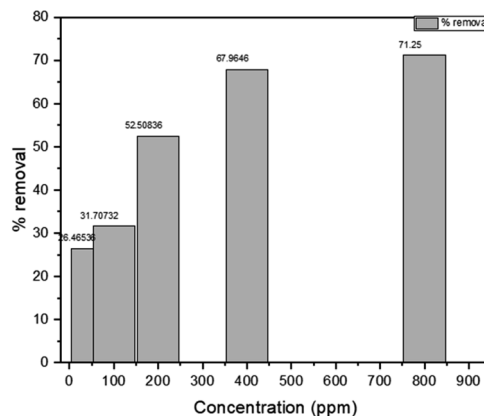


**Fig. 13** The effect of concentration of drug was investigated under constant conditions, including a drug concentration of 800 ppm, an adsorbent dose of 30 mg, a pH of 7, and a temperature of 65 °C for 180 minutes.
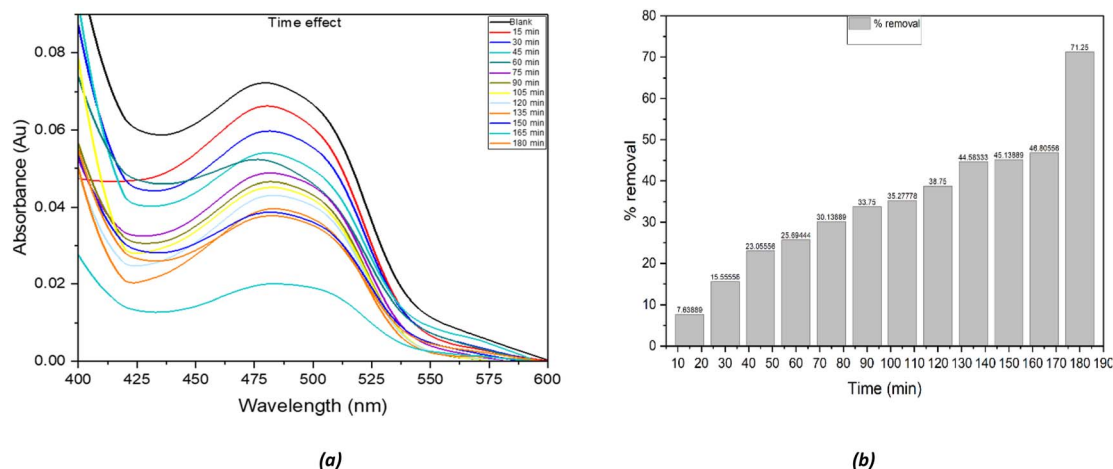


**Fig. 12** (a) The effect of contact time on the removal of the drug was investigated under constant conditions, including a drug concentration of 800 ppm, an adsorbent dose of 30 mg, a pH of 7, and a temperature of 65 °C, (b) bar graph of adsorption of Piracetam at various contact time.
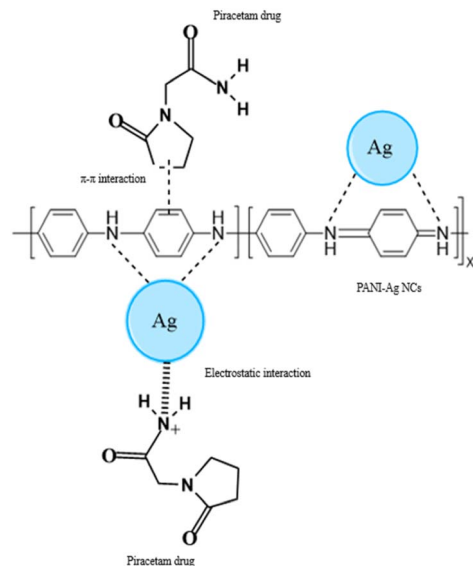
Fig. 14 A schematic diagram of the adsorption mechanism for effective drug removal by PANI-Ag NCs.



Fig. 15 Langmuir isotherm plot for the removal of Piracetam drug by synthesized PANI-Ag NCs.

interface.[56] Two isotherm models were applied to understand the type of interaction: (i) the Langmuir isotherm model and (ii) the Freundlich isotherm model. Langmuir model suggests that monolayer adsorption occurs throughout the process and there is no interaction between the adsorbed particles. Freundlich model assumes that multilayer adsorption occurs due to the interaction between the adsorbed particles.[58,59]

The suitability of the isotherm to describe the adsorption process was assessed using the correlation coefficient $R^2$. The linear plot of $C_e/q_e$ against $C_e$ indicates that the Langmuir isotherm is applicable. The values of $q_{max}$ and $K_L$ are obtained from the slope and intercept of this plot, as per Equation

$$\frac{c_e}{q_e} = \frac{1}{K_L q_{max}} + \frac{c_e}{q_{max}}$$

$C_e$ represents the equilibrium concentration of the drug in solution (mg L$^{-1}$), $q_e$ is the amount of drug adsorbed on the surface of polyaniline-coated silver nanocomposites at equilibrium (mg g$^{-1}$), $q_{max}$ is the maximum adsorption capacity for a monolayer, and $K_L$ is the adsorption energy (L g$^{-1}$).

Adsorption isotherms describe the equilibrium relationship between adsorbate concentration in solution and its adsorption onto the nanocomposite surface. The Langmuir and Freundlich models were used to interpret adsorption behavior.

**6.1.1. Langmuir isotherm.** The Langmuir model assumed monolayer adsorption on a homogenous surface with finite adsorption sites. The linearized Langmuir equation was used to calculate the maximum adsorption capacity ($q_{max}$) and adsorption energy ($K_L$). The experimental data fitted well with the Langmuir model, as indicated by a high correlation coefficient ($R^2$ close to 1), suggesting uniform adsorption and no significant interaction between adsorbed molecules. The maximum adsorption capacity ($q_{max}$) was 63.2 mg g$^{-1}$, which aligns with values reported for PANI-based nanocomposites in similar studies.

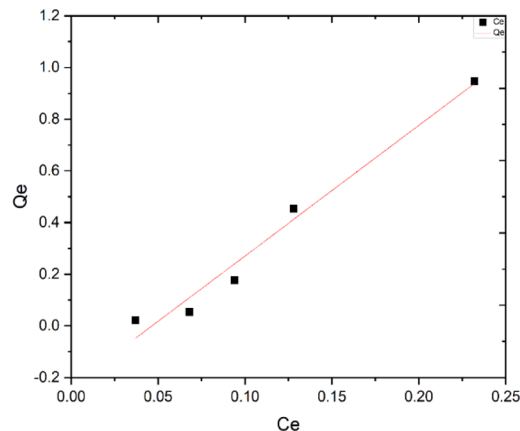Fig. 15 had depicted the Langmuir isotherm plot, which had established the relationship between the equilibrium concentration of piracetam in the solution ($C_e$) and the amount adsorbed per unit mass of the adsorbent ($q_e$). The linearity of the plot had confirmed that the adsorption of piracetam onto PANI-Ag nanocomposites had followed the Langmuir model, indicating monolayer adsorption on a homogeneous surface. The derived parameters, including the maximum adsorption capacity ($q_{max}$) and the Langmuir constant ($K_L$), had highlighted the high adsorption efficiency of the nanocomposites. The strong correlation coefficient ($R^2$) had supported the applicability of the Langmuir model, suggesting that the active sites on the adsorbent surface had been uniform and equally accessible. These findings had concluded that the adsorption process had been highly effective and primarily governed by monolayer adsorption mechanisms.

**6.1.2. Freundlich isotherm.** The Freundlich model accounts for multi-layer adsorption on heterogeneous surfaces. The Freundlich constants ($K_F$ and $n$) indicated optimized adsorption, with an $n$ value between 1 and 10, supporting strong adsorbate–adsorbent interactions. This model demonstrated slightly lower $R^2$ values compared to the Langmuir model, suggesting that while multilayer adsorption occurred, monolayer adsorption predominated.

The Freundlich isotherm accounts for adsorption in heterogeneous systems and is not limited to monolayer formation. The Freundlich equation is expressed as:

$$\ln q_e = \ln K_F + \left(\frac{1}{n}\right)\ln C_e$$

Fig. 16 had illustrated the Freundlich isotherm plot, showing the logarithmic relationship between the equilibrium concentration ($C_e$) and adsorption capacity ($q_e$). Unlike the Langmuir isotherm, the Freundlich model had accounted for the heterogeneity of the adsorbent's surface, allowing multilayer adsorption. The calculated Freundlich constants, $K_F$ (adsorption capacity) and $n$ (adsorption intensity), had revealed the varying affinities of the nanocomposites' surface. The value of $n$, within

© 2025 The Author(s). Published by the Royal Society of Chemistry

*Environ. Sci.: Adv.*, 2025, **4**, 1250–1266 | **1261**

the favourable range of 1–10, had indicated a beneficial adsorption process. However, the Freundlich model's lower correlation coefficient compared to the Langmuir model had suggested that monolayer adsorption had dominated, with heterogeneity playing a secondary role. Thus, while the surface of the PANI-Ag nanocomposites had exhibited some degree of heterogeneity, the adsorption process had been primarily uniformed and efficient.

Similar adsorption capacities have been reported for PANI-based adsorbents, such as 58.6 mg g$^{-1}$ for Cr(VI) removal and 60 mg g$^{-1}$ for methylene blue adsorption. The alignment with the Langmuir isotherm has also been observed in studies using Ag-PANI nanocomposites for dye and heavy metal removal, reinforcing the findings here.[60]

Thus, in conclusion, the adsorption isotherms accurately described the process, with a predominant Langmuir fit suggesting monolayer adsorption on a homogenous surface. The high $q_{max}$ value indicates excellent adsorption efficiency, validating the use of PANI-Ag nanocomposites.

### 6.2. Adsorption kinetics

Kinetic analysis was carried out to understand the adsorption dynamic and mechanism. Three models, pseudo-first-order, pseudo-second-order, and intra-particle diffusion, were evaluated.

**6.2.1. Pseudo-first-order mode.** The pseudo-first-order model suggests that the adsorption efficiency is directly proportional to the number of active sites available on the adsorbent surface, implying physical adsorption or physisorption. The model is stated by the following equation:

$$\ln(q_e - q_t) = \ln q_e - K_1 t$$

$k_1$ is the first-order adsorption rate constant. Calculation of pseudo-first order rate constant $k_1$ and equilibrium adsorption amount $q_e$ can be done by plotting $\log(q_e - q_t)$ as a function of time $t$. From the slope and intercept of this plot, the value of $k_1$ and $q_e$ can be derived.
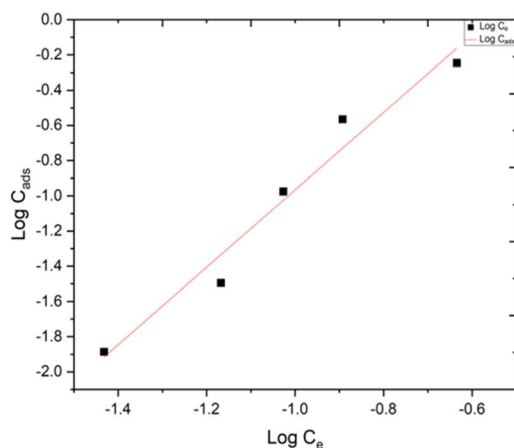


**Fig. 16** Freundlich isotherm Plot for the removal of Piracetam drug by synthesized PANI–Ag NCs.

A $\ln(q_e - q_t)$ *vs.* time plot determined the rate constant ($k_1$) and equilibrium adsorption capacity ($q_e$). The model showed a moderate fit, indicating that physical adsorption (physisorption) alone does not fully explain the process.

**6.2.2. Pseudo-second-order model.** The pseudo second-order model suggests that the adsorption efficiency is based on the amount of drug molecules adsorbed at any time and at equilibrium. This infers chemical adsorption (chemisorption) of the process. The following equation illustrates the model:

$$\frac{t}{q_t} = \frac{1}{k_2 q_e^2} + \frac{t}{q_e}$$

This model assumes chemisorption as the rate-determining step, where adsorption occurs *via* valence forces or electron sharing. The pseudo-second-order kinetics model shows a very strong correlation value ($R^2 = 0.999$), indicating that the adsorption process follows a reaction rate that is directly proportional to the square of the number of adsorbed molecules. This suggests that the adsorption process is likely influenced by chemical interaction between the adsorbate and adsorbent, rather than by physical adsorption alone. A linear plot of $t/q_t$ *versus* time confirmed an excellent fit ($R^2$ close to 1). The pseudo-second-order rate constant ($k_2$) and $q_e$ values closely matched experimental results, confirming that chemisorption played a dominant role in the process.

*5.2.2.3. Intra-particle diffusion model.* This model examined the diffusion of drug molecules within the pores of the adsorbent. A multi-linear plot indicated that the adsorption process involved multiple stages, including both external mass transfer and intra-particle diffusion. The absence of a straight-line origin intercept suggested that while intra-particle diffusion was significant, other factors like surface adsorption contributed to the overall mechanism.

Similar trends have been reported for Ag-PANI nanocomposites in the removal of pharmaceuticals and dyes, with pseudo-second-order kinetics dominating the process. In studies involving heavy metal adsorption using PANI nanocomposites, the chemisorption mechanism was also predominant, reinforcing the findings of this study. The kinetic studies confirmed that chemisorption is the primary mechanism driving the adsorption process. The pseudo-second-order model provided the optimal fit, aligning with literature and supporting the effectiveness of PANI-Ag nanocomposites for piracetam removal.

Fig. 17 and 18 had evaluated the adsorption kinetics of piracetam removal through pseudo-first-order and pseudo-second-order kinetics. The pseudo-first-order plot, which had assumed physical adsorption (physisorption), had exhibited a lower correlation coefficient, suggesting that physisorption had not been the dominant mechanism. In contrast, the pseudo-second-order plot, based on chemisorption, had provided an excellent fit with a high $R^2$ value. This model had assumed that the adsorption efficiency was directly related to the square of the number of available active sites, implying the formation of strong chemical interaction between the adsorbent and the adsorbate. These findings had confirmed that the
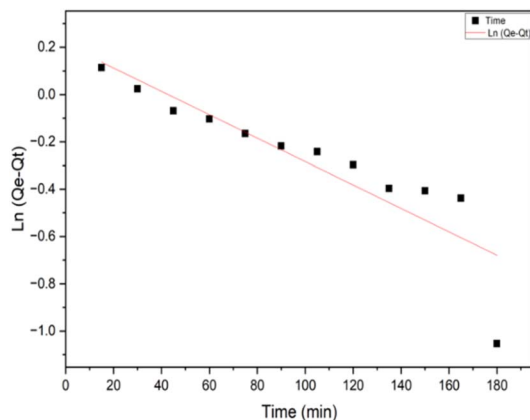
**Fig. 17** The plot showing kinetics of pseudo first-order for removal of piracetam drug by PANI-Ag NCs; 50 ml, 0.8 g L$^{-1}$ adsorbent, at 65 °C, steering speed 1000 rpm and pH 7 for 180 minutes.

adsorption process had been primarily governed by chemisorption, with the PANI-Ag nanocomposites providing specific active sites that had facilitated strong interactions with piracetam molecules. The results had highlighted the high efficiency and reliability of these nanocomposites in environmental remediation applications.

The adsorption studies had demonstrated that the removal of piracetam by PANI-Ag nanocomposites had followed the Langmuir isotherm, confirming monolayer adsorption on a homogeneous surface. The adsorption process had been dominated by chemisorption, as evidenced by the pseudo-second-order kinetics. While the Freundlich isotherm had indicated some degree of surface heterogeneity, its lower applicability had underscored the uniformity and high efficiency of the adsorbent. Collectively, these findings had validated the potential of PANI-Ag nanocomposites as effective, reliable, and environmentally friendly adsorbents for pharmaceutical pollutant removal. Although this study focused on removal, the PANI-Ag nanocomposites may also have potential
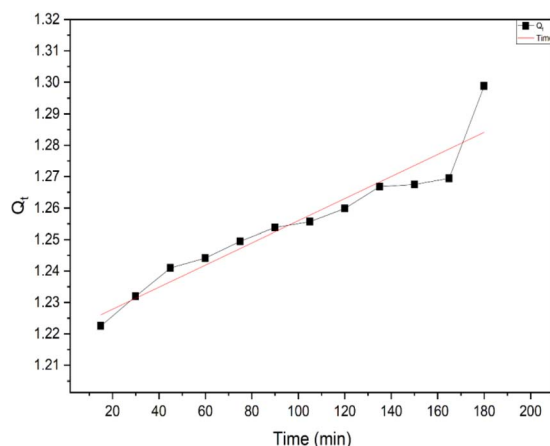


**Fig. 18** The plot showing kinetics of pseudo-second-order for removal of piracetam drug by PANI-Ag NCs; 50 ml, 0.8 g per L adsorbent, at 65 °C, steering speed 1000 rpm and pH 7 for 180 minutes.

for sustained drug release applications.[61] However, the potential toxicity of silver nanoparticles within these composites requires thorough evaluation, especially for environmental and biomedical uses, highlighting the necessity for further toxicological evaluation.

## Conclusions

This study successfully synthesized PANI-Ag nanocomposites *via* an unreported eco-friendly, plant-mediated method using garlic extract, representing a novel approach for the adsorption of Piracetam. Characterization techniques (UV-Vis, FTIR, DLS, Zeta Potential, SEM-EDX, HRTEM, and XRD) confirmed their stability and successful synthesis. The nanocomposites demonstrated excellent adsorption efficiency for Piracetam, making them promising candidates for drug removal applications. Additionally, their significant antioxidant activity highlights potential applications in environmental remediation and biomedical fields. Future research should focus on optimizing synthesis conditions to enhance their performance in large-scale applications.

## Data availability

All data generated or analyzed during this study are included in this published article and its ESI files.†

## Author contributions

Conceptualization, methodology, software, writing—original draft preparation, P. K.; supervision, validation, formal analysis, investigation, writing—review and editing, R. B.; A. P.; resources, project administration, data curation, R. S.; all authors have read and agreed to the published version of the manuscript.

## Conflicts of interest

There are no conflicts to declare.

## Acknowledgements

## Notes and references

1 A. Sandoval, C. Hernández-Ventura and T. E. Klimova, Titanate nanotubes for removal of methylene blue dye by combined adsorption and photocatalysis, *Fuel*, 2017, **198**, 22–30.

2 M. Kampa and E. Castanas, Human health effects of air pollution, *Environ. Pollut.*, 2008, **151**(2), 362–367.

3 J. Huang, S. Tan, P. D. Lund and H. Zhou, Impact of H 2 O on organic–inorganic hybrid perovskite solar cells, *Energy Environ. Sci.*, 2017, **10**(11), 2284–2311.

4 J. Ma, J. Shi, H. Ding, G. Zhu, K. Fu and X. Fu, Synthesis of cationic polyacrylamide by low-pressure UV initiation for turbidity water flocculation, *Chem. Eng. J.*, 2017, **312**, 20–29.

5 G. Zhu, J. Liu, J. Yin, Z. Li, B. Ren, Y. Sun, P. Wan and Y. Liu, Functionalized polyacrylamide by xanthate for Cr (VI) removal from aqueous solution, *Chem. Eng. J.*, 2016, **288**, 390–398.

6 J. Yin, G. Zhu and B. Deng, Graphene oxide (GO) enhanced polyamide (PA) thin-film nanocomposite (TFN) membrane for water purification, *Desalination*, 2016, **379**, 93–101.

7 G. Zhu, Y. Bian, A. S. Hursthouse, P. Wan, K. Szymanska, J. Ma, X. Wang and Z. Zhao, Application of 3-D fluorescence: characterization of natural organic matter in natural water and water purification systems, *J. Fluoresc.*, 2017, **27**, 2069–2094.

8 G. Zhu, Q. Wang, J. Yin, Z. Li, P. Zhang, B. Ren, G. Fan and P. Wan, Toward a better understanding of coagulation for dissolved organic nitrogen using polymeric zinc-iron-phosphate coagulant, *Water Res.*, 2016, **100**, 201–210.

9 G. Zhu, J. Liu and Y. Bian, Evaluation of cationic polyacrylamide-based hybrid coagulation for the removal of dissolved organic nitrogen, *Environ. Sci. Pollut. Res.*, 2018, **25**, 14447–14459.

10 F. M. Christensen, Pharmaceuticals in the environment—a human risk?, *Regul. Toxicol. Pharmacol.*, 1998, **28**(3), 212–221.

11 C. A. Kinney, E. T. Furlong, S. L. Werner and J. D. Cahill, Presence and distribution of wastewater-derived pharmaceuticals in soil irrigated with reclaimed water, *Environ. Toxicol. Chem.*, 2006, **25**(2), 317–326.

12 K. K. Sadasivuni, S. Rattan, S. Waseem, S. K. Brahme, S. B. Kondawar, S. Ghosh, A. P. Das, P. K. Chakraborty, J. Adhikari, P. Saha and P. Mazumdar, Silver nanoparticles and its polymer nanocomposites—Synthesis, optimization, biomedical usage, and its various applications, *Polymer Nanocomposites in Biomedical Engineering*, 2019, pp. 331–373.

13 I. Ali, H. Y. Aboul-Enein, and K. Kümmerer, Analyses of drugs and pharmaceuticals in the environment, in *Biophysico-Chemical Processes of Anthropogenic Organic Compounds in Environmental Systems*, 2011, pp. 439–462.

14 M. J. Ahmed and B. H. Hameed, Removal of emerging pharmaceutical contaminants by adsorption in a fixed-bed column: a review, *Ecotoxicol. Environ. Saf.*, 2018, **149**, 257–266.

15 L. Wang, X. Zhao, J. Zhang and Z. Xiong, Selective adsorption of Pb (II) over the zinc-based MOFs in aqueous solution-kinetics, isotherms, and the ion exchange mechanism, *Environ. Sci. Pollut. Res.*, 2017, **24**, 14198–14206.

16 M. C. Gutierrez, M. Pepió and M. Crespi, Electrochemical oxidation of reactive dyes: method validation and application, *Color. Technol.*, 2002, **118**(1), 1–5.

17 V. C. Taty-Costodes, H. Fauduet, C. Porte and A. Delacroix, Removal of Cd (II) and Pb (II) ions, from aqueous solutions, by adsorption onto sawdust of Pinus sylvestris, *J. Hazard. Mater.*, 2003, **105**(1–3), 121–142.

18 D. Mahanta, G. Madras, S. Radhakrishnan and S. Patil, Adsorption of sulfonated dyes by polyaniline emeraldine salt and its kinetics, *J. Phys. Chem. B*, 2008, **112**(33), 10153–10157.

19 C. Giurgea, *The "Nootropic" Approach to the Pharmacology of the Integrative Activity of the Brain 1, 2. Conditional Reflex: a Pavlovian Journal of Research & Therapy*, 1973, vol. 8, pp. 108–115.

20 S. Ullah, R. Khalid, M. F. Rehman, M. I. Irfan, A. Abbas, A. Alhoshani, F. Anwar and H. M. Amin, Biosynthesis of phyto-functionalized silver nanoparticles using olive fruit extract and evaluation of their antibacterial and antioxidant properties, *Front. Chem.*, 2023, **11**, 1202252.

21 V. V. Singh, Green nanotechnology for environmental remediation, in *Sustainable Nanotechnology for Environmental Remediation*, Elsevier, 2022, pp. 31–61.

22 M. Mosaviniya, T. Kikhavani, M. Tanzifi, M. T. Yaraki, P. Tajbakhsh and A. Lajevardi, Facile green synthesis of silver nanoparticles using Crocus Haussknechtii Bois bulb extract: Catalytic activity and antibacterial properties, *Colloid Interface Sci. Commun.*, 2019, **33**, 100211.

23 A. C. Burdușel, O. Gherasim, A. M. Grumezescu, L. Mogoantă, A. Ficai and E. Andronescu, Biomedical applications of silver nanoparticles: an up-to-date overview, *Nanomaterials*, 2018, **8**(9), 681.

24 C. Graf, D. L. Vossen, A. Imhof and A. van Blaaderen, A general method to coat colloidal particles with silica, *Langmuir*, 2003, **19**(17), 6693–6700.

25 A. Jabbar, A. Abbas, N. Assad, M. Naeem-ul-Hassan, H. A. Alhazmi, A. Najmi, K. Zoghebi, M. Al Bratty, A. Hanbashi and H. M. Amin, A highly selective Hg 2+ colorimetric sensor and antimicrobial agent based on green synthesized silver nanoparticles using Equisetum diffusum extract, *RSC Adv.*, 2023, **13**(41), 28666–28675.

26 F. A. Rajathi, C. Parthiban, V. G. Kumar and P. Anantharaman, Biosynthesis of antibacterial gold nanoparticles using brown alga, Stoechospermum marginatum (kützing), *Spectrochim. Acta, Part A*, 2012, **99**, 166–173.

27 A. Abbas, M. A. Hussain, M. Amin, M. N. Tahir, I. Jantan, A. Hameed and S. N. Bukhari, Multiple cross-linked hydroxypropylcellulose–succinate–salicylate: prodrug design, characterization, stimuli responsive swelling–deswelling and sustained drug release, *RSC Adv.*, 2015, **5**(54), 43440–43448.

28 A. Abbas and H. M. Amin, Silver nanoparticles modified electrodes for electroanalysis: An updated review and a perspective, *Microchem. J.*, 2022, **175**, 107166.

29 K. Toplak Galle, *Domaće Ljekovito Bilje*, Mozaik knjiga, Zagreb, 2005.

30 C. Borek, Garlic reduces dementia and heart-disease risk, *J. Nutr.*, 2006, **136**(3), 810S–812S.

31 C. Borek, Antioxidant health effects of aged garlic extract, *J. Nutr.*, 2001, **131**(3), 1010S–1015S.

32 R. Prakash, R. Bharti, A. Thakur, M. Verma and R. Sharma, Environmentally Benign Green Approach for the Synthesis of IONPs Using Vicia Faba Fruit Extract and Their Antioxidant Activities, *Sustainable Chem. Eng.*, 2025, 11–21.

33 V. Saini, A. Thakur, M. Verma, R. Bharti and R. Sharma, Biosynthesis of CoNPs: An Overview, *Orbital:Electron. J. Chem.*, 2024, **31**, 293–305.

34 P. Kaushik, R. Bharti, R. Sharma, M. Verma, R. T. Olsson and A. Pandey, Progress in synthesis and applications of Polyaniline-Coated Nanocomposites: A comprehensive review, *Eur. Polym. J.*, 2024, **15**, 113574.

35 A. Yadav and R. Bharti, Gold Nanoparticles in Cancer Treatment and Diagnostics: A Review of Emerging Trends and Therapeutic Potential, *Orbital:Electron. J. Chem.*, 2024, **16**, 205–218.

36 A. Singh, R. Bharti, A. Thakur, M. Verma and R. Sharma, Leaf Extract Mediated Green Synthesis of Iron-oxide Nanoparticles (FeO-NPs) by Using Hibiscus rosa-sinensis (China rose): A Potential Approach and its Biological Application, *Orbital:Electron. J. Chem.*, 2024, 271–278.

37 S. Bansal, R. Bharti, A. Thakur, M. Verma and R. Sharma, Synthesis and Characterization of Iron Oxide Nanoparticles by Using Callistemon viminalis Flowers Extract: An Eco-Friendly Approach with Promising Antioxidant Activities, *Orbital:Electron. J. Chem.*, 2024, 240–246.

38 A. Thakur, M. Verma, R. Bharti and R. Sharma, Recent advancement in the green synthesis of silver nanoparticles, *Curr. Chin. Sci.*, 2023, **3**(5), 322–348.

39 M. Ates, T. Karazehir and A. J. Sezai Sarac, Conducting polymers and their applications, *Curr. Phys. Chem.*, 2012, **2**(3), 224–240.

40 V. K. Gupta, A. Nayak, S. Agarwal and I. Tyagi, Polyaniline and its composites for environmental applications: A review, *Environ. Sci. Pollut. Res.*, 2012, **19**(8), 2900–2926.

41 K. Gopalakrishnan, C. Ramesh, V. Ragunathan and M. Thamilselvan, Antibacterial activity of Cu2O nanoparticles on E. coli synthesized from Tridax procumbens leaf extract and surface coating with polyaniline, *Digest J. Nanomater. Biostruct.*, 2012, **7**(2), 833–839.

42 S. Singh, A. Bharti and V. K. Meena, Green synthesis of multi-shaped silver nanoparticles: Optical, morphological and antibacterial properties, *J. Mater. Sci.: Mater. Electron.*, 2015, **26**(6), 3638–3648.

43 A. Verma and T. Kumar, Gas sensing properties of a Cu-doped PANI nanocomposite towards ammonia, *Mater. Adv.*, 2024, **5**(18), 7387–7400.

44 A. Y. Arasi, J. J. Jeyakumari, B. Sundaresan, V. Dhanalakshmi and R. Anbarasan, The structural properties of poly (aniline)—analysis via FTIR spectroscopy, *Spectrochim. Acta, Part A*, 2009, **74**(5), 1229–1234.

45 X. S. Du, C. F. Zhou and Y. W. Mai, Facile synthesis of hierarchical polyaniline nanostructures with dendritic nanofibers as scaffolds, *J. Phys. Chem. C*, 2008, **112**(50), 19836–19840.

46 S. Jayasudha, L. Priya and K. T. Vasudevan, Structural, optical and electrical characterization of polyaniline/silver nanocomposites, *Int. J. Res. Eng. Technol.*, 2016, **5**, 1–6.

47 M. Rezvani, A. A. Asgharinezhad, H. Ebrahimzadeh and N. Shekari, A polyaniline-magnetite nanocomposite as an anion exchange sorbent for solid-phase extraction of chromium (VI) ions, *Microchim. Acta*, 2014, **181**, 1887–1895.

48 D. S. Patil, J. S. Shaikh, S. A. Pawar, R. S. Devan, Y. R. Ma, A. V. Moholkar, J. H. Kim, R. S. Kalubarme, C. J. Park and P. S. Patil, Investigations on silver/polyaniline electrodes for electrochemical supercapacitors, *Phys. Chem. Chem. Phys.*, 2012, **14**(34), 11886–11895.

49 A. Ali, M. A. Hussain, A. Abbas, T. A. Khan, G. Muhammad, M. T. Haseeb and I. Azhar, Comparative isoconversional thermal analysis and degradation kinetics of Salvia spinosa (Kanocha) seed hydrogel and its acetates: A potential matrix for sustained drug release, *Cellul. Chem. Technol.*, 2022, **56**(3–4), 239–250.

50 D. S. Patil, J. S. Shaikh, S. A. Pawar, R. S. Devan, Y. R. Ma, A. V. Moholkar, J. H. Kim, R. S. Kalubarme, C. J. Park and P. S. Patil, Investigations on silver/polyaniline electrodes for electrochemical supercapacitors, *Phys. Chem. Chem. Phys.*, 2012, **14**(34), 11886–11895.

51 S. Ebrahim, A. Shokry, M. M. Khalil, H. Ibrahim and M. Soliman, Polyaniline/Ag nanoparticles/graphene oxide nanocomposite fluorescent sensor for recognition of chromium (VI) ions, *Sci. Rep.*, 2020, **10**(1), 13617.

52 S. Amin, M. Sher, A. Ali, M. F. Rehman, A. Hayat, M. Ikram, A. Abbas and H. M. Amin, Sulfonamide-functionalized silver nanoparticles as an analytical nanoprobe for selective Ni (II) sensing with synergistic antimicrobial activity, *Environ. Nanotechnol., Monit. Manage.*, 2022, **18**, 100735.

53 N. Assad, M. Naeem-ul-Hassan, M. Ajaz Hussain, A. Abbas, M. Sher, G. Muhammad, Y. Assad and M. Farid-ul-Haq, Diffused sunlight assisted green synthesis of silver nanoparticles using Cotoneaster nummularia polar extract for antimicrobial and wound healing applications, *Nat. Prod. Res.*, 2025, **39**(8), 2203–2217.

54 S. Mohebali, D. Bastani and H. Shayesteh, Methylene blue removal using modified celery (Apium graveolens) as a low-cost biosorbent in batch mode: kinetic, equilibrium, and thermodynamic studies, *J. Mol. Struct.*, 2018, **1173**, 541–551.

55 E. M. Soliman, S. A. Ahmed and A. A. Fadl, Reactivity of sugar cane bagasse as a natural solid phase extractor for selective removal of Fe (III) and heavy-metal ions from natural water samples, *Arabian J. Chem.*, 2011, **4**(1), 63–70.

56 A. Ali, M. A. Hussain, A. Z. Abbas, T. A. Khan, G. Muhammad, M. T. Haseeb and I. Azhar, Comparative isoconversional thermal analysis and degradation kinetics of Salvia spinosa (Kanocha) seed hydrogel and its acetates: a potential matrix for sustained drug release, *Cellul. Chem. Technol.*, 2022, **56**, 239–250.

57 M. I. Irfan, F. Amjad, A. Abbas, M. F. Rehman, F. Kanwal, M. Saeed, S. Ullah and C. Lu, Novel carboxylic acid-capped silver nanoparticles as antimicrobial and colorimetric sensing agents, *Molecules*, 2022, **27**(11), 3363.

© 2025 The Author(s). Published by the Royal Society of Chemistry

*Environ. Sci.: Adv.*, 2025, **4**, 1250–1266 | **1265**

58 W. Wang, X. Yang, Y. Fang and J. Ding, Preparation and performance of form-stable polyethylene glycol/silicon dioxide composites as solid–liquid phase change materials, *Appl. Energy*, 2009, **86**(2), 170–174.

59 R. S. Azarudeen, M. A. Riswan Ahamed, R. Subha and A. R. Burkanudeen, Heavy and toxic metal ion removal by a novel polymeric ion-exchanger: synthesis, characterization, kinetics and equilibrium studies, *J. Chem. Technol. Biotechnol.*, 2015, **90**(12), 2170–2179.

60 G. Joseph, S. D. Pai, A. Varghese, D. Pinheiro, M. K. Mohan and S. J. Chundattu, Adsorptive capacity of PANI/Bi2O3 composite through isotherm and kinetics studies on alizarin red, *J. Mol. Struct.*, 2024, **1308**, 138095.

61 M. A. Abbas, F. Bashir, A. Abbas and M. Rizwan, Synthesis, Characterization, and Stimuli Responsive On/Off Switching of Cross-Linked Hydroxyethyl Starch: A Smart Material for Intelligent Drug Delivery, *Starch-Stärke*, 2022, **74**(11–12), 2100199.